HHS Public Access

Author manuscript

Biochem Pharmacol. Author manuscript; available in PMC 2021 January 28.

Published in final edited form as:

Biochem Pharmacol. 2017 May 15; 132: 29–37. doi:10.1016/j.bcp.2017.02.019.

Selective reversal of BCRP-mediated MDR by VEGFR-2 inhibitor ZM323881

Yun-Kai Zhang[a], **Xiao-Yu Zhang**[a], **Guan-Nan Zhang**[a], **Yi-Jun Wang**[a], **Huizhong Xu**[b,1], **Dongmei Zhang**[c], **Suneet Shukla**[d,2], **Lili Liu**[e], **Dong-Hua Yang**[a], **Suresh V. Ambudkar**[d], **Zhe-Sheng Chen**[a,*]

[a]College of Pharmacy and Health Sciences, St. John's University, Queens, NY 11439, USA

[b]College of Liberal Arts and Sciences, St. John's University, Queens, NY 11439, USA

[c]College of Pharmacy, Jinan University, Guangzhou 510632, China

[d]Laboratory of Cell Biology, Center for Cancer Research, National Cancer Institute, National Institutes of Health, Bethesda, MD 20892, USA

[e]Guangdong Province Hospital for Occupational Disease Prevention and Treatment, Guangzhou 510300, China

Abstract

The expression of breast cancer resistant protein (BCRP) in lung cancer is correlated with development of multidrug resistance (MDR) and therefore leads to lower response to chemotherapy. ZM323881, a previously developed selective VEGFR-2 inhibitor, was found to have inhibitory effects on BCRP-mediated MDR in this investigation. ZM323881 significantly decreased the cytotoxic doses of mitoxantrone and SN-38 in BCRP-overexpressing NCI-H460/MX20 cells. Mechanistic studies revealed that ZM323881 effected by inhibiting BCRP-mediated drug efflux, leading to intracellular accumulation of BCRP substrates. No significant alteration in the expression levels and localization pattern of BCRP was observed when BCRP-overexpressing cells were exposed to ZM323881. Stimulated bell-shaped ATPase activities were observed. Molecular docking suggested that ZM323881 binds to the modulator site of BCRP and the binding pose is stable validated by 100 ns molecular dynamic simulation. Overall, our results indicated that ZM323881 reversed BCRP-related MDR by inhibiting its efflux function. These findings might be useful in developing combination chemotherapy for MDR cancer treatment.

Keywords

Lung cancer; Multidrug resistance; BCRP; ZM323881

*Corresponding author at: 8000 Utopia Parkway, Queens, NY 11439, USA., chenz@stjohns.edu (Z.-S. Chen).
[1]Present address: Department of Physics and Astronomy, San Francisco State University, San Francisco, CA 94132, USA.
[2]Present address: Division of Biopharmaceutics, Office of New Drug Products, Office of Pharmaceutical Quality, Center for Drug Evaluation and Research, Food and Drug Administration, Silver Spring, Maryland, USA.

Conflicts of interest

The authors declare no conflict of interest.

1. Introduction

Non-small cell lung cancer (NSCLC) accounts for 80–85% of lung cancer and is the leading cause of cancer morbidity and mortality worldwide with a 5-year survival rate of 15% [1,2]. The majority of patients with lung cancer developed distant metastatic at the time of diagnosis, making it hard to use surgery and radiation as therapeutic options. Also, despite successful surgical resection, the recurrence rate remains high [3]. Though it was believed the chemotherapy can lead to therapeutic effectiveness and longer survival rate, such strategies often inaugurate cancer cells to evade cell death by a phenomenon known as multidrug resistance [4].

Multidrug resistance (MDR) is defined as the insensitivity of cells to cytotoxic actions of a number of structurally and functionally unrelated drugs. MDR in cancer cells poses a major challenge to the clinicians and pharmacologists to effectively treat cancers by chemotherapeutic agents. In the past few decades many research efforts were devoted to understanding the mechanisms by which cancer cells develop MDR. Some of these mechanisms, such as reduced uptake of drugs, cell cycle arrest, altered drug target, increased efflux of drugs and sequestration of drugs in lysosomes have since been identified [5,6]. The most prominent cause of MDR is the increased efflux of anti-cancer drugs by ATPbinding cassette (ABC) transporters [7]. ABC transporters were named as a conserved intracellular ATP binding domain provides the energy required for conformational changes in the transmembrane domain, which effectively pump out substrates across the cell membrane [7,8]. Breast cancer resistance protein (BCRP/ABCG2/MXR) is the second member of the G subfamily of ABC transporter superfamily. BCRP has its unique features, which contains only one nucleotide-binding domain (NBD) and one transmembrane domain (TMD). It has been widely accepted that a functional ABC transporter requires at least two TMDs and two NBDs to form a central substrate translocation pathway. Therefore, BCRP is likely to form a homodimer or homooligomer in order to be functional [9]. A number of chemotherapeutic agents have been shown to be transported by BCRP. BCRP expression phenotype was described to be resistant to mitoxantrone, 9-aminocamptothecin, topotecan, irinotecan and SN-38 (the active metabolite of irinotecan) [10].

As a prognostic indicator for lung cancer, the expression of BCRP is correlated with lower overall survival, shorter progression-free survival and lower response to therapy in NSCLC [11,12]. Therefore, blocking BCRP is an effective way to restore chemosensitivity in MDR NSCLC cells. In addition to the potential therapeutic relevance, developing and understanding of new specific modulators of BCRP will be beneficial in understanding BCRP function [13]. Unfortunately, few clinically useful inhibitors of BCRP have been developed. The fungal toxin fumitremorgin C (FTC), isolated from *Aspergillus fumigatus*, is a potent and specific inhibitor of BCRP, but its CNS neurotoxic effects preclude its clinical use [14]. The tetracyclic FTC analogue Ko143 was found to be unstable in plasma [15]. Therefore, new specific BCRP inhibitor is still needed.

Vascular endothelial growth factor (VEGF) is produced by most tumor types and stimulates the process of angiogenesis [16], playing a significant role in establishing a vascular supply within the tumor. All lung cancers aberrantly express VEGF, therefore its pathway is

targeted by therapeutic regimens of lung cancer [17]. Dual inhibition of VEGF receptor and BCRP was therefore proposed to be beneficial in lung cancers. In this study, we determined whether ZM323881, a previously developed selective VEGFR-2 inhibitor, could reverse BCRP-related MDR in NSCLC and other cancer cells.

2. Materials and methods

2.1. Reagents

ZM323881 was kindly provided as samples from Selleck Chemicals (Houston, TX). Dulbecco's modified Eagle's Medium (DMEM), penicillin/streptomycin and trypsin 0.25% were purchased from Corning Life Sciences (Tewksbury MA). Fetal bovine serum (FBS) and bovine calf serum were purchased from Hyclone (GE Healthcare Life Science, Pittsburgh, PA). Mitoxantrone, SN-38, and cisplatin were products from Medkoo Biosciences, Inc. (Chapel Hill, NC). Fumitremorgin C (FTC) was a gift from Dr. Susan Bates (NIH, Bethesda, MD). Monoclonal antibody BXP-21 (against BCRP) was purchased from GeneTex (Irvine, CA). Monoclonal antibody BA3R (against β-actin), Alexa Fluor 488 conjugated goat anti-mouse IgG secondary antibody, HRP-conjugated rabbit anti-mouse secondary antibody and RNase A were purchased from Thermo Fisher Scientific Inc. (Waltham, MA). [^{3}H]-mitoxantrone (2.5 Ci/mmol) were purchased from Moravek Biochemicals, Inc. (Brea, CA).

2.2. Cell lines and cell culture

Human non-small lung cancer cell line NCI-H460 and its mitoxantrone-resistant BCRP-overexpressing NCI-H460/MX20 cells, human colon cancer cell line SW620 and its doxorubicin-resistance P-gp-overexpressing SW620/Ad300 cells were kindly provided by Drs. Susan Bates and Robert Robey (NIH, Bethesda, MD). HEK293/pcDNA3.1, HEK/ABCG2-R482, HEK/ABCG2-R482G and HEK/ABCG2-R482T were established previously by transfecting either empty vector pcDNA3.1 (HEK293/pcDNA3.1) or vector with insert of wild-type human *ABCG2* gene (HEK/ABCG2-R482) or mutant *ABCG2* gene (HEK/ABCG2-R482G or HEK/ABCG2-R482T). All the cell lines were grown as adherent monolayers in poly-D-lysine coated flasks with DMEM supplemented with 10% FBS or bovine calf serum and 1% penicillin/streptomycin in a humidified incubator containing 5% CO_2 at 37 °C.

2.3. Cytotoxicities by MTT assay

Modified MTT colorimetric assay was used to measure the changes of cytotoxicities of anticancer drugs with or without inhibitors. Cells were seeded into coated 96-well microplates and were cultured overnight. ZM323881 or FTC were added 1 h prior to chemotherapeutic drugs. After 72 h of incubation, 20 μL of MTT in PBS solution (4 mg/mL) was added into each well, then the microplates were further incubated for 4 h in dark. The culture medium was then aspirated and 100 μL of DMSO was added to dissolve the formazan. The $A_{570\ nm}$ was measured by the Multiskan™ GO microplate spectrophotometer (Thermo Fisher, Waltham, MA). IC_{50} values were calculated using the modified Bliss method.

2.4. Hoechst 33342 accumulation and fluorescence microscopic analysis

Cells were grown in coated 6-well plates and washed two times with phosphate-buffered saline (PBS). ZM323881 was added to cells at the final concentration of 10 μM and the cells were incubated at 37 °C for 60 min. Hoechst 33342 (4 μg/mL) was then added directly to each well, and the cells were further incubated for 60 min at 37 °C. After Hoechst staining, cells were maintained at 4 °C before fluorescence microscopic analysis.

2.5. [^{3}H]-mitoxantrone intracellular accumulation and efflux assay

Cells were trypsinized, washed, and resuspended at 10^6 cells/mL in complete culture medium. Cells were pre-incubated with either PBS, ZM323881 (5 and 10 μM) or FTC (5 μM) for 1 h. Subsequently, cells were incubated in the complete culture medium containing 0.01 nM [^{3}H]-mitoxantrone for 2 h in the presence of above treatment. After washing two times with ice-cold PBS, the cells were pelleted and lysed. The cell lysates were placed in 5 mL liquid scintillation cocktail and the radioactivity was counted in the Packard TRI-CARB 1900CA liquid scintillation analyzer (Packard Instrument, Downers Grove, IL) as previously described [18].

To study the [^{3}H]-mitoxantrone efflux, the cells were incubated sequentially with [^{3}H]-mitoxantrone containing medium for 2 h (accumulation phase), and then drug-free medium for another 2 h (efflux phase). Serial aliquots at 0, 30, 60 and 120 min in efflux phase were taken and washed with ice-cold PBS. The samples were analyzed as previously described in accumulation assay. To study the effects of reversal agents on the time course of [^{3}H]-mitoxantrone efflux, ZM323881 and FTC were added to each phase respectively.

2.6. Western blotting and immunofluorescence of BCRP

After treatment with 10 μM ZM323881 for 24, 48 and 72 h, the cells were incubated with lysis buffer (10 mM Tris, 1 mM EDTA, 0.1% SDS, 150 mM NaCl, 1% Triton-X and protease inhibitor cocktail) on ice for 20 min, followed by centrifugation at 12,000g at 4 °C for 15 min. The supernatant was collected and the protein concentration was determined by bicinchoninic acid (BCA) based protein assay (Thermo Scientific, Waltham, MA). Forty μg of protein (80 μg protein for NCI-H460 lysate) was separated by SDS-polyacrylamide gel electrophoresis and transferred to a polyvinylidene difluoride membrane. The blot was probed with primary antibody BXP-21 (1:500, detects BCRP) and BA3R (1:500, detects β-actin) followed by HRP-conjugated secondary antibodies. The signal was detected using enhanced chemiluminescence. The protein expression was quantified by ImageJ software (NIH, Bethesda, MD, USA).

For immunofluorescence assay, the cells were grown in poly-D-lysine coated coverslips and treated with or without 10 μM ZM323881 for 72 h. The cells were then washed and fixed in formaldehyde, permeabilized by 0.1% Triton X-100 and then blocked using 6% BSA. Monoclonal antibody BXP-21 (1:400) followed by Alexa Fluor 488 conjugated secondary antibody (1:2000) was used to localize BCRP. Cells were mounted using Pro-Long® Gold Antifade Mountant (Thermo Scientific, Waltham, MA), with DAPI and then examined by fluorescence microscopy.

2.7. BCRP ATPase assay

The BCRP ATPase assay was performed as previously described [19]. Briefly, the BCRP membrane vesicles were incubated in ATPase assay buffer with or without vanadate for 5 min at 37 °C. ZM323881 or mitoxantrone were then added to the assay buffer in concentration gradient and incubated for 3 min 37 °C. MgATP was then added to assay buffer and the mixture was incubated for 20 min at 37 °C. The reactions were stopped by adding SDS. The ATPase activity due to the BCRP transporter is calculated from the amount of inorganic phosphate determined by colorimetry.

2.8. BCRP Induced-Fit docking and molecular dynamics (MD) simulation

Human BCRP homology model and docking grid was prepared and defined as previously described [19]. The structures of ZM323881, mitoxantrone and SN-38 were built and prepared by Ligprep v3.3 module (Schrödinger, Cambridge, MA, USA, 2015). The energy minimized compounds were subjected to Glide XP (extra precision) docking (Glide v6.6, Schrödinger, Cambridge, MA, USA, 2015). In order to study the effects of mutations of residue 482 in ZM323881 binding, different mutations were generated in Maestro by editing the BCRP docking grid. Prepared structure of ZM323881 was then subjected to Glide XP docking on wild-type and mutant BCRP. At the transmembrane site of BCRP, the best scored ZM323881 pose from XP run was used to generate the starting grid for induced-fit docking (IFD) calculation. The default Glide extensive sampling IFD protocol was followed and the docking score (kcal/mol) was calculated.

The docked ZM323881-BCRP (wild-type) complex was then subjected to long MD simulation for validation. The system was prepared in Maestro with the POPC bilayer and explicit TIP3P waters added. Periodic boundary condition with 15 Å buffer distance was applied so that the complex does not directly interact with its own periodic image. Counter-ions were added to neutralize the overall charge of the system. The MD simulation was performed via Desmond v4.5 in the NPT ensemble (1.015 bar and 300 K) using a time step of 2 fs. The default protocol was applied to equilibrate the system (8 stages, 160 ps). The equilibrated complex system was then subjected to 100,000 ps (100 ns) MD simulation. The coordinates were saved every 10 ps and the root mean square deviation (RMSD) was calculated using the first frame as reference. All calculations were performed on a 6-core Xeon processor except MD simulation was performed on a Nvidia GPU.

2.9. Fluorescence microscopy

Fluorescence images were collected using a Nikon TE-2000S microscope with an APO 20× air lens and APO 60× oil immersion lens (Nikon). Fluorescence from Hoechst 33342 and DAPI was excited and collected with Nikon UV-2E/C filter combination. Alexa Fluor 488 fluorescence was excited and collected with Nikon B1-E filter combination. The same fluorescence settings (excitation, lamp power, detector gain and exposure) were used to image different samples.

2.10. Statistics

All experiments were prepared at least three times and the differences were determined by one-way ANOVA. Differences were considered significant when $p < 0.05$.

3. Results

3.1. ZM323881 significantly sensitized NCI-H460/MX20 cells to mitoxantrone and SN-38, but not cisplatin

As compared to parental NCI-H460 cells, the drug selected NCI-H460/MX20 cells exhibited significant multidrug resistance to mitoxantrone and SN-38 due to overexpressing of BCRP as previously described. In order to determine the reversal effect of ZM323881, non-toxic concentrations of ZM323881 were applied to cells as chemosensitizer prior to chemotherapeutical agents. As shown in Fig. 1A and B, ZM323881 at 5 and 10 μM significantly sensitized NCI-H460/MX20 cells to mitoxantrone and SN-38. ZM323881 at 10 μM decreased mitoxantrone IC_{50} from 28.3 μM to 0.76 μM. Compared with parental NCI-H460 cells, the resistance-fold of mitoxantrone in NCI-H460/MX20 was decreased from 217.6-fold to 6.3-fold by 10 μM of ZM323881. Similarly, ZM323881 sensitized NCI-H460/MX20 cells to SN-38 from IC_{50} value 11.6 μM to 0.86 μM (128.9-fold to 10.8-fold as compared to parental cells). In the meantime, ZM323881 did not sensitize parental NCI-H460 cells to either mitoxantrone or SN-38. A known BCRP inhibitor, FTC at 5 μM, was used as a positive control chemosensitizer. As shown in Fig. 1C, NCI-H460/MX20 cells were not resistant to cisplatin as compared to NCI-H460 cells, and neither FTC nor ZM323881 significantly altered the IC_{50} values to cisplatin in parental and resistant cells.

3.2. ZM323881 did not sensitize SW620/Ad300 cells to doxorubicin

As shown in Fig. 1D, the IC_{50} values of doxorubicin in SW620/Ad300 cells were 183.2-fold higher than that in SW620 cells. Verapamil at 10 μM significantly decreased the doxorubicin IC_{50} values in SW620/Ad300 cells, reversing doxorubicin resistance from 183.2-fold to 1.54-fold. However, ZM323881 did not significantly decrease the doxorubicin IC_{50} at both 5 and 10 μM.

3.3. Effects of ZM323881 on wild-type and mutant BCRP transfected cells

The mutations at Arg482 have been reported to be crucial for the substrate and inhibitor specificity of BCRP. Therefore, in order to study the effects of ZM323881 on both wild-type (R482) and mutant (R482G and R482T) BCRP, different stable transfected cells were used in the present study. As shown in Fig. 2A and B, in comparison to empty vector transfected HEK293/pcDNA3.1 cells, BCRP-transfected HEK/ABCG2-R482, HEK/ABCG2-R482G and HEK/ABCG2-R482T cells exhibited multidrug resistances to mitoxantrone and SN-38. Similarly, applications of ZM323881 at 5 and 10 μM could significantly decrease the IC_{50} values and therefore reversed the MDR.

In order to compare the reversal effects of ZM323881 on wild-type or mutant BCRP, we calculated the percentage dose remaining after BCRP inhibition for mitoxantrone and SN-38 as shown in Fig. 2C and D. BCRP inhibition by both FTC and ZM323881 did not significantly alter the doses of mitoxantrone and SN-38 in HEK293/pcDNA3.1 cells. However, ZM323881 at 10 μM leads to 90.7% dose reduction in HEK/ABCG2-R482, 90.9% dose reduction in HEK/ABCG2-R482G and 92.2% dose reduction in HEK/ABCG2-R482T cells for mitoxantrone. Similarly, only 16.1% SN-38 dose for HEK/ABCG2-R482, 9.5% SN-38 dose for HEK/ABCG2-R482G and 7.7% SN-38 dose for HEK/ABCG2-R482T were

required to reach IC_{50} after BCRP inhibition by 10 μM ZM323881. The inhibitory effects of ZM323881 on BCRP followed a concentration dependent pattern.

3.4. Effects of ZM323881 on Hoechst 33342 accumulation

It has been previously reported that BCRP is an efficient Hoechst 33342 efflux pump, therefore Hoechst 33342 could be used as a probe for evaluation of BCRP function. Fluorescence microscopy (Fig. 3A) revealed that Hoechst 33342 fluorescence was greater in NCI-H460 cells compared with NCI-H460/MX20 cells. Moreover, in NCI-H460/MX20 cells, instead of a nucleus-bound pattern, a membrane-bound fluorescence pattern was observed, suggesting the efflux role of BCRP. The treatment of ZM323881 did not change the intensity or the intracellular pattern of Hoechst 33342 fluorescence in NCI-H460 cells. However, treatment of NCI-H460/MX20 cells with ZM323881 increased the fluorescence intensity significantly. The intracellular localization of Hoechst 33342 fluorescence in ZM323881-treated resistant cells was similar to that in the parental cells.

3.5. Effects of ZM323881 on [^{3}H]-mitoxantrone accumulation

In order to quantify the intracellular accumulation of BCRP substrate, [^{3}H]-mitoxantrone accumulation was measured in parental and BCRP-mediated MDR cells with or without inhibitors. As shown in Fig. 3B, lower intracellular [^{3}H]-accumulation was observed in resistant NCI-H460/MX20 cells compared to parental NCI-H460 cells. Pretreatment of 10 μM ZM323881 increased the intracellular [^{3}H]-mitoxantrone in NCI-H460/MX20 cells from 32.9% to 96.2% of that in parental cells. FTC was used as positive control for BCRP inhibition. ZM323881 and FTC also slightly increased the [^{3}H]-mitoxantrone accumulation level in NCI-H460 cells.

3.6. Effects of ZM323881 on the efflux of [^{3}H]-mitoxantrone

Drug efflux can occur as a result of passive diffusion and also active transport by specific pumps. In order to quantify the time-course of drug efflux in parental and BCRP-mediated MDR cells, a [^{3}H]-mitoxantrone efflux assay was performed. As shown in Fig. 3C, untreated NCI-H460 cells effluxed 24% of the normalized intracellular [^{3}H]-mitoxantrone in 120 min. ZM323881 and FTC treatments increased the retention of [^{3}H]-mitoxantrone, however the difference is not significant. While in untreated MDR NCI-H460/MX20 cells (Fig. 3D), 61% of the normalized intracellular [^{3}H]-mitoxantrone was effluxed within 120 min of incubation. BCRP inhibition with ZM323881 at 5 and 10 μM resulted in significantly increased [^{3}H]-mitoxantrone intracellular retention (74.4% and 81.0% respectively).

3.7. Effects of ZM323881 on the expression level and intracellular localization of BCRP

Western blot was used to determine the effects of ZM323881 on the expression level of BCRP. As shown in Fig. 4A and B, treatment of NCI-H460/MX20 up to 72 h did not significantly alter the expression level of BCRP. Therefore, ZM323881 might not sensitize NCI-H460/MX20 cells by down-regulating BCRP. We further visualized intracellular localization of BCRP inside NCI-H460/MX20 cells using immunofluorescence assay (Fig. 4C). Membrane enriched fluorescent signals was observed, consistent with the role of BCRP

as a membrane-bound efflux pump. The treatment of ZM323881 did not have significant effects on the intracellular localization of BCRP.

3.8. BCRP ATPase assays

The effects of ZM323881 and mitoxantrone on BCRP ATPase were measured by ATP hydrolysis in the presence of drugs at different concentrations from 0 to 40 μM. Both ZM323881 and mitoxantrone stimulated the BCRP ATPase activity. As shown in Fig. 4D and E, ZM323881 stimulated BCRP ATPase with a maximal stimulation of 3.18-fold of the basal activity, while mitoxantrone stimulated BCRP ATPase with a maximal 2.04-fold of the basal activity.

3.9. ZM323881-BCRP molecular docking and molecular dynamics

As previously reported, the conformational changes of protein may allow the protein to generate close conformations to the shape of the ligand and therefore lead to better binding affinity complex. In this study, the induced-fit docking was carried out to study the interactions between ZM323881 and human homology BCRP. As shown in Fig. 5A, the best-scored docked poses of ZM323881 were predicted at the same location within the transmembrane domain through hydrophobic interactions with nearby residues for both wild-type and R482-mutant BCRP. ZM323881 exhibited a Glide score of −10.770 kcal/mol on wild-type BCRP model (Fig. 5B). A π-π interaction was predicted between the benzyloxy group of ZM323881 and indole ring of Trp627. The ligand quinazoline ring formed another π-π interaction with the phenyl ring of Phe551. Two hydrogen bonds were formed between the phenolic group of ZM323881 and His630. For R482G mutant BCRP, ZM323881 exhibited a Glide score of −10.584 kcal/mol (Fig. 5C). The quinazoline ring of ZM323881 formed a π-π interaction with the indole group of Trp627. The phenolic group of ZM323881 formed a hydrogen bond with the phenolic group of Tyr570. For R482T mutant (Fig. 5D), the Glide score is −11.509 kcal/mol for docked ZM323881 and mutant BCRP complex. The phenyl ring of ligand benzyloxy group formed two π-π interactions with indole ring of Trp627 and the imidazole ring of His630. The ligand quinazoline ring formed another π-π interaction with Trp627. The nitrogen atom of ligand quinazoline ring formed a hydrogen bond with the phenolic group of Tyr576. The ligand phenolic group formed a hydrogen bond with the amide group of Asn584.

We further performed molecular docking for BCRP substrate mitoxantrone and SN-38. As shown in Fig. 5E, the docked poses of mitoxantrone and SN-38 are located in a distinct position as compared to ZM323881 pose. In order to validate the docked pose, a molecular dynamics simulation was carried out for ZM323881-BCRP (wild-type) for 100 ns. The superimposition of ZM323881 in pre- and post-MD complex is depicted in Fig. 5F. The binding pocket did not have significant changes and the ligand is still within the binding pocket. Also, monitoring the RMSD can indicate if the simulation has equilibrated. As shown in Fig. 5G, the backbone of protein in the complex deviated up to 8 Å in the first 4 ns, then it acquired a stable conformation and persisted until the end of simulation. Small fluctuations of ZM323881 was observed in the first 50 ns of simulation with a RMSD up to 2.2 Å, indicating these fluctuations of the ligand were inside the binding pocket.

4. Discussion

Although VEGFR-1 and VEGFR-2 expressions were observed previously in NCI-H460 cells [20], the addition of ZM323881 alone did not inhibit the cell proliferation in our results. Similarly, there are other reports that neutralizing the VEGFR using monoclonal antibody Bevacizumab (Avastin®) did not produce any inhibitory effects in NCI-H460 cells as compared with IgG control antibody [21]. A possible explanation is that NCI-H460 lacks expression of neuropilin-1 and neuropilin-2, which are important co-receptors to VEGF [21,22]. Although ZM323881 did not suppress NCI-H460 cells, in this study, we discovered the sensitizing effects ZM323881 on MDR cells, which could be helpful in developing more potent combinational chemotherapy for targeted lung cancer patients.

The sensitizing effects of ZM323881 on NCI-H460/MX20 cells were clearly related to BCRP through our experimental design for the following reasons. First, ZM323881 did not significantly sensitize parental NCI-H460 cells, in which BCRP is not over-expressed as shown in our Western blot results. Second, cisplatin is not a substrate of BCRP therefore the IC_{50} values of cisplatin is similar in parental NCI-H460 and NCI-H460/MX20 cells. ZM323881 did not sensitize these cells towards cisplatin, suggesting the sensitizing effects of ZM323881 is limited to BCRP-substrates. Moreover, ZM323881 did not sensitize P-gp-overexpressing SW620/Ad300 cells towards doxorubicin although doxorubicin is a moderate substrate of BCRP. This is because the hypothesized ZM323881 target BCRP is missing in SW620/Ad300 cells. Last, ZM323881 exhibited similar reversal effects on BCRP-transfected cells, in which BCRP is the sole contributor to drug resistance. Overall, we concluded that ZM323881 sensitized MDR cells by targeting BCRP transporter.

Furthermore, BCRP was previously reported as an active efflux pump. Therefore, inhibition of BCRP would lead to decreased drug efflux, increased drug accumulation and in turn increased drug efficacy. Our drug efflux assay showed the accelerated drug efflux in BCRP-overexpressing cells and the inhibition of ZM323881 on BCRP resulted in significant decrease in drug efflux. Reduced drug efflux is not a guarantee for intracellular drug accumulation especially in cancer cells, since the drugs may be deactivated due to altered metabolic pathways [23]. Therefore, Hoechst 33342 and [^{3}H]-mitoxantrone were used to directly show the intracellular drug accumulation qualitatively and quantitatively. These results indicated that the mechanism of ZM323881 in sensitizing BCRP overexpressing MDR cells is that ZM323881 inhibits the efflux function of BCRP, resulting in elevated intracellular drug accumulation which leads to cell death.

As a membrane-bound transporter, BCRP might lose its function by being down-regulated or translocated into cytoplasm. Since 1-h of pretreatment of ZM32381 exhibited sufficient inhibitory effects to BCRP, it is not likely that the inhibitory effects were related to down-regulation. This hypothesis was examined by our Western blotting analysis. No obvious down-regulation of BCRP was observed after the cells were treated with ZM323881 up to 72 h. Therefore, ZM323881 did not function as a BCRP down-regulator. It is noted that parental NCI-H460 cells also have detectable BCRP expression. This BCRP expression may explain the insignificant reversal effect of ZM323881 on NCI-H460. Translocation of membrane transporter can happen in milliseconds [24], However our immunofluorescence

assay did not prove BCRP translocation. Taking all these results into consideration, we conclude that ZM323881 directly targets BCRP to inhibit its function.

BCRP, as an ABC transporter, use ATP as energy source to transport substrates across cell membranes. The BCRP ATPase activity can be detected as the amount of inorganic phosphate released by BCRP. ZM323881 had a ‘bell shaped’ curve while mitoxantrone exhibited a Michaelis-Menten type curve in inducing ATPase activity of BCRP. The possible explanation for the ‘bell-shape’ is a two binding site model. It has been previously reported that two distinct binding sites, the modulator site (M-site) and the substrate-binding H/R sites exist in ABC transporter [25]. If the affinities of the two binding sites are very different, the Michaelis-Menten type curves are usually observed. If the two binding affinities are close to each other the curve is bell-shaped [26]. It is then hypothesized from the ATPase that ZM323881 may have stronger affinity to the modulator site of BCRP, while mitoxantrone binds to the substrate site. Our molecular docking also predicted that ZM323881 has a distinct binding site as compared to BCRP substrate mitoxantrone and sN-38 (Fig. 5E). Moreover, ZM323881 exhibited high glide gscore (near −11 kcal/mol) towards both wild-type and mutant BCRP at that binding site, suggesting strong affinities. This may explain the phenomenon that the effectiveness of ZM323881 is not sensitive towards R482 mutations in BCRP. Besides, several previous studies have revealed the problem that some well-docked ligand might ‘fly’ away from the binding pocket in MD simulations [27,28]. Our post-docking validation MD simulation indicated BCRP is quickly equilibrated in about 5 ns simulation, and the binding site which is composed of resides in transmembrane helixes also did not change significantly (Fig. 5F). ZM323881 binding pose is very stable (RMSD about 2 Å) through 100 ns.

In conclusion, this study reports that ZM323881 reverses BCRP-mediated MDR by binding at the modulator site of BCRP, inhibiting its efflux function and increasing intracellular drug concentrations. These results suggest that in targeted patients with VEGFR-2 positive and BCRP positive MDR, ZM323381’s dual function against VEGFR-2 and BCRP may be beneficial to inhibiting VEGF-related angiogenesis and also to augmenting the clinical response to chemotherapies.

Acknowledgements

We thank Selleck Chemicals (Houston, TX) for providing sample of ZM323881. We are thankful to Drs. Susan E. Bates and Robert W. Robey (NIH, MD) for FTC, SW620, SW620/Ad300, ABCG2-transfected cell lines, NCI-H460 and NCI-H460/MX20 cells lines. We thank Dr. Mark F. Rosenbery (University of Manchester, Manchester, UK) and Dr. Zsolt Bikádi (Virtua Drug Ltd., Budapest, Hungary) for providing human BCRP homology model. We thank Dr. Tanaji T. Talele (St. John’s University, New York) for providing the computational resources of induced-fit dockings. This work was supported by funds from NIH (No. 1R15CA143701 and No. 1R15GM116043-01) and St. John’s University Research Seed Grant (No. 579-1110-7002) to Z. Chen. S.S and S.V.A were supported by the Intramural Research Program of National Institutes of Health, National Cancer Institute, Center for Cancer Research.

References

[1]. Breathnach OS, Freidlin B, Conley B, Green MR, Johnson DH, Gandara DR, O’Connell M, Shepherd FA, Johnson BE, Twenty-two years of phase III trials for patients with advanced non-small-cell lung cancer: sobering results, J. Clin. Oncol. 19 (6) (2001) 1734–1742. [PubMed: 11251004]

[2]. Bareschino MA, Schettino C, Rossi A, Maione P, Sacco PC, Zeppa R, Gridelli C, Treatment of advanced non small cell lung cancer, J. Thorac. Dis. 3 (2) (2011) 122–133. [PubMed: 22263075]

[3]. Uramoto H, Tanaka F, Recurrence after surgery in patients with NSCLC, Transl. Lung Cancer Res. 3 (4) (2014) 242–249. [PubMed: 25806307]

[4]. Amiri-Kordestani L, Basseville A, Kurdziel K, Fojo AT, Bates SE, Targeting MDR in breast and lung cancer: discriminating its potential importance from the failure of drug resistance reversal studies, Drug Resist. Updates 15 (1–2) (2012) 50–61.

[5]. Wu Q, Yang Z, Nie Y, Shi Y, Fan D, Multi-drug resistance in cancer chemotherapeutics: mechanisms and lab approaches, Cancer Lett. 347 (2) (2014) 159–166. [PubMed: 24657660]

[6]. Li W, Zhang H, Assaraf YG, Zhao K, Xu X, Xie J, Yang DH, Chen ZS, Overcoming ABC transporter-mediated multidrug resistance: Molecular mechanisms and novel therapeutic drug strategies, Drug Resist. Updates 27 (2016) 14–29.

[7]. Zhang YK, Wang YJ, Gupta P, Chen ZS, Multidrug Resistance Proteins (MRPs) and Cancer Therapy, AAPS J. 17 (4) (2015) 802–812. [PubMed: 25840885]

[8]. Schmitt L, Tampe R, Structure and mechanism of ABC transporters, Curr. Opin. Struct. Biol. 12 (6) (2002) 754–760. [PubMed: 12504680]

[9]. Ni Z, Bikadi Z, Rosenberg MF, Mao Q, Structure and function of the human breast cancer resistance protein (BCRP/ABCG2), Curr. Drug Metab. 11 (7) (2010) 603–617. [PubMed: 20812902]

[10]. Robey RW, Polgar O, Deeken J, To KW, Bates SE, ABCG2: determining its relevance in clinical drug resistance, Cancer Metastasis Rev. 26 (1) (2007) 39–57. [PubMed: 17323127]

[11]. Li F, Zeng H, Ying K, The combination of stem cell markers CD133 and ABCG2 predicts relapse in stage I non-small cell lung carcinomas, Med. Oncol. 28 (4) (2011) 1458–1462. [PubMed: 20717756]

[12]. Hang D, Dong HC, Ning T, Dong B, Hou DL, Xu WG, Prognostic value of the stem cell markers CD133 and ABCG2 expression in esophageal squamous cell carcinoma, Dis. Esophagus 25 (7) (2012) 638–644. [PubMed: 22236447]

[13]. Henrich CJ, Robey RW, Bokesch HR, Bates SE, Shukla S, Ambudkar SV, Dean M, McMahon JB, New inhibitors of ABCG2 identified by high-throughput screening, Mol. Cancer Ther. 6 (12 Pt 1) (2007) 3271–3278. [PubMed: 18089721]

[14]. Allen JD, van Loevezijn A, Lakhai JM, van der Valk M, van Tellingen O, Reid G, Schellens JH, Koomen GJ, Schinkel AH, Potent and specific inhibition of the breast cancer resistance protein multidrug transporter in vitro and in mouse intestine by a novel analogue of fumitremorgin C, Mol. Cancer Ther. 1 (6) (2002) 417–425. [PubMed: 12477054]

[15]. Weidner LD, Zoghbi SS, Lu S, Shukla S, Ambudkar SV, Pike VW, Mulder J, Gottesman MM, Innis RB, Hall MD, The inhibitor Ko143 is not specific for ABCG2, J. Pharmacol. Exp. Ther. 354 (3) (2015) 384–393. [PubMed: 26148857]

[16]. Hicklin DJ, Ellis LM, Role of the vascular endothelial growth factor pathway in tumor growth and angiogenesis, J. Clin. Oncol. 23 (5) (2005) 1011–1027. [PubMed: 15585754]

[17]. Alevizakos M, Kaltsas S, Syrigos KN, The VEGF pathway in lung cancer, Cancer Chemother. Pharmacol. 72 (6) (2013) 1169–1181. [PubMed: 24085262]

[18]. Zhang YK, Zhang H, Zhang GN, Wang YJ, Kathawala RJ, Si R, Patel BA, Xu J, Chen ZS, Semi-synthetic ocotillol analogues as selective ABCB1-mediated drug resistance reversal agents, Oncotarget 6 (27) (2015) 24277–24290. [PubMed: 26296969]

[19]. Zhang YK, Zhang GN, Wang YJ, Patel BA, Talele TT, Yang DH, Chen ZS, Bafetinib (INNO-406) reverses multidrug resistance by inhibiting the efflux function of ABCB1 and ABCG2 transporters, Sci. Rep. 6 (2016) 25694. [PubMed: 27157787]

[20]. Jang YJ, Kim DS, Jeon OH, Kim DS, Saxatilin suppresses tumor-induced angiogenesis by regulating VEGF expression in NCI-H460 human lung cancer cells, J. Biochem. Mol. Biol. 40 (3) (2007) 439–443. [PubMed: 17562297]

[21]. Barr MP, Gray SG, Gately K, Hams E, Fallon PG, Davies AM, Richard DJ, Pidgeon GP, O'Byrne KJ, Vascular endothelial growth factor is an autocrine growth factor, signaling through neuropilin-1 in non-small cell lung cancer, Mol. Cancer 14 (2015) 45. [PubMed: 25889301]

[22]. Hong TM, Chen YL, Wu YY, Yuan A, Chao YC, Chung YC, Wu MH, Yang SC, Pan SH, Shih JY, Chan WK, Yang PC, Targeting neuropilin 1 as an antitumor strategy in lung cancer, Clin. Cancer Res. 13 (16) (2007) 4759–4768. [PubMed: 17699853]

[23]. Herling A, Konig M, Bulik S, Holzhutter HG, Enzymatic features of the glucose metabolism in tumor cells, FEBS J. 278 (14) (2011) 2436–2459. [PubMed: 21564549]

[24]. Winterfeld S, Ernst S, Borsch M, Gerken U, Kuhn A, Real time observation of single membrane protein insertion events by the Escherichia coli insertase YidC, PLoS ONE 8 (3) (2013) e59023. [PubMed: 23527078]

[25]. Ferreira RJ, Ferreira MJ, dos Santos DJ, Molecular docking characterizes substrate-binding sites and efflux modulation mechanisms within P-glycoprotein, J. Chem. Inf. Model. 53 (7) (2013) 1747–1760. [PubMed: 23802684]

[26]. Al-Shawi MK, Polar MK, Omote H, Figler RA, Transition state analysis of the coupling of drug transport to ATP hydrolysis by P-glycoprotein, J. Biol. Chem. 278 (52) (2003) 52629–52640. [PubMed: 14551217]

[27]. Chen KC, Chen HY, Chen CY, Potential Protein Phosphatase 2A Agents from Traditional Chinese Medicine against Cancer, Evid Based Complement Altern. Med. 2014 (2014) 436863.

[28]. Chen YC, Beware of docking!, Trends Pharmacol Sci. 36 (2) (2015) 78–95. [PubMed: 25543280]

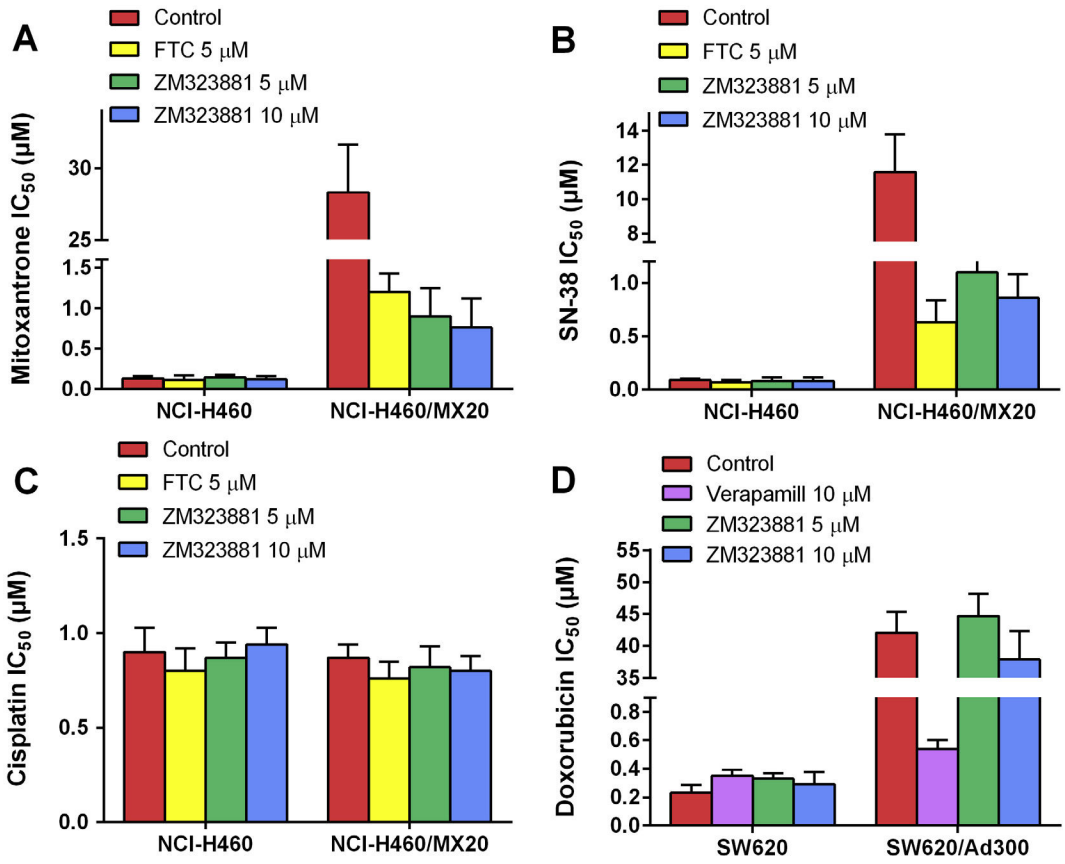

Fig. 1.

Effects of ZM323881 on the IC_{50} values of (A) mitoxantrone, (B) SN-38 and (C) cisplatin in parental NCI-H460 and drug-selected BCRP-overexpressing multidrug resistant NCI-H460/MX20 cells. Effects of ZM323881 on the IC_{50} values of (D) doxorubicin in parental SW620 and drug-selected PGP-overexpressing multidrug resistant SW620/Ad300 cells. Error bars represent SD. FTC 5 μM or verapamil 10 μM is used as positive control for BCRP or PGP-overexpressing cells respectively.

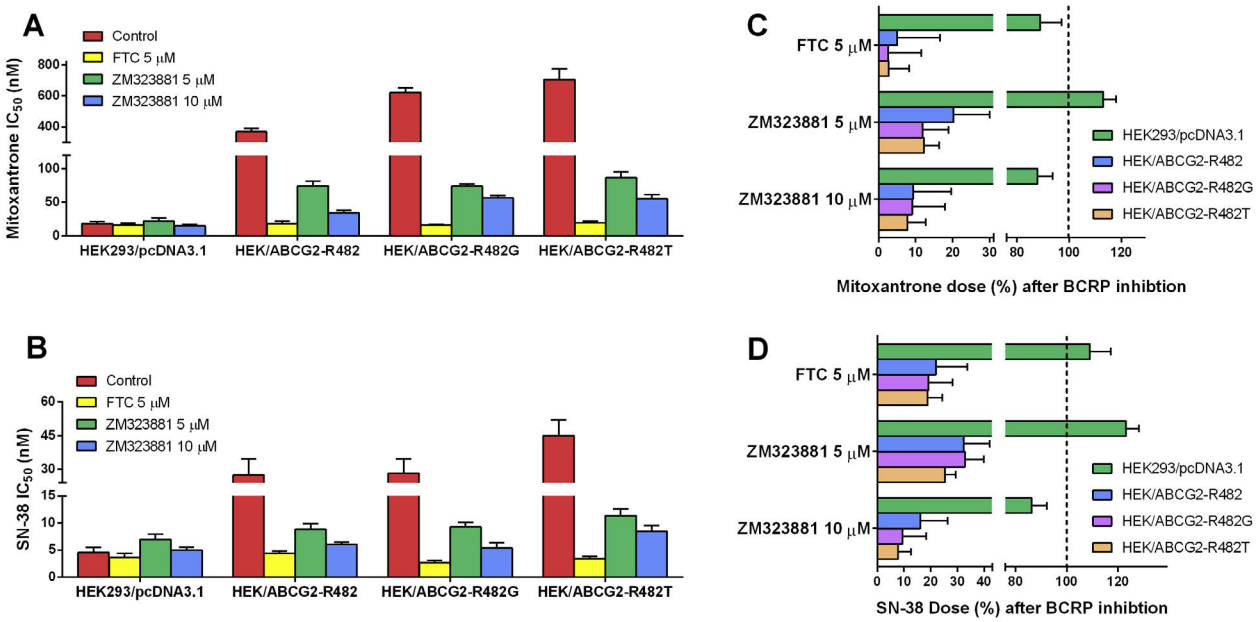

Fig. 2.

Effects of ZM323881 on the IC_{50} values of (A) mitoxantrone and (B) SN-38 in parental HEK293/pcDNA3.1 and transfected BCRP-overexpressing HEK/ABCG2-R482, HEK/ABCG2-R482G and HEK/ABCG2-R482T cells. The percentage dose remaining for (C) mitoxantrone and (D) SN-38 after BCRP inhibition to reach IC_{50} in parental and BCRP-transfected cells. Dashed lines show the mitoxantrone or SN-38 dose prior to BCRP inhibition (100%). Error bars represent the SD. FTC 5 μM is used as positive control for BCRP inhibition.

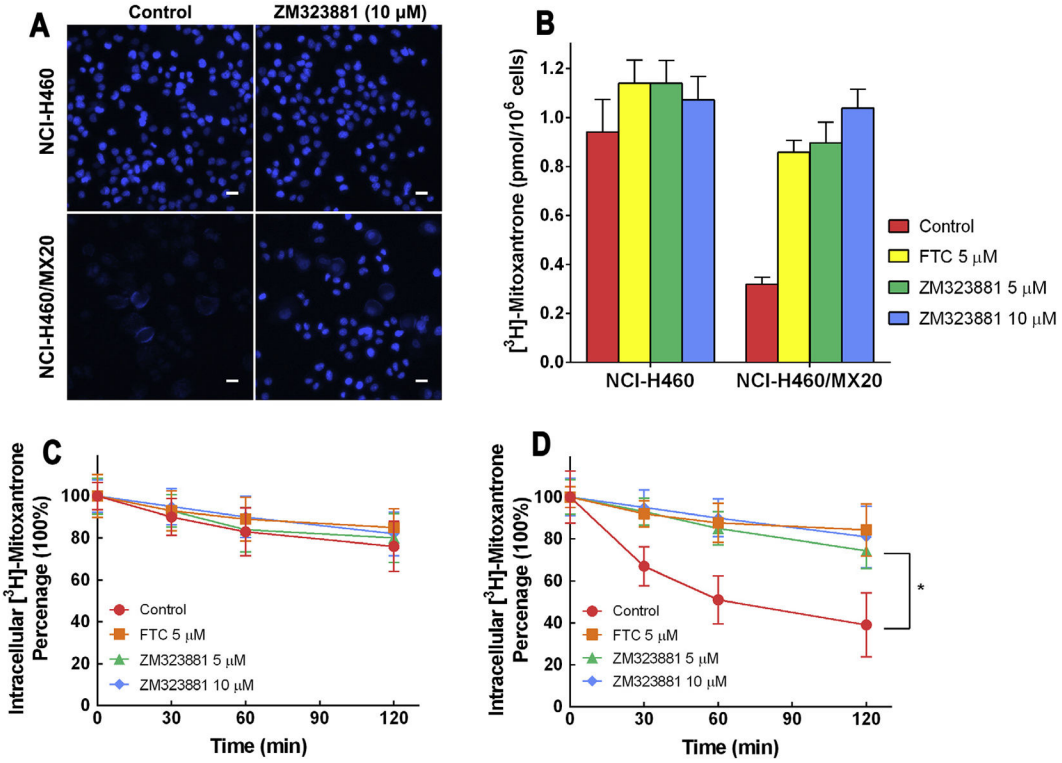

Fig. 3.

(A) Fluorescence microscopic analysis of Hoechst 33342 staining of NCI-H460 and NCI-H460/MX20 cells. Cells were treated as described in '2. Materials and Methods'. Scale bar, 10 μm. (B) Effects of ZM323881 on intracellular accumulation of [^{3}H]-mitoxantrone in NCI-H460 and NCI-H460/MX20 cells. (C) Efflux of [^{3}H]-mitoxantrone in the absence and presence of inhibitors in NCI-H460 cells. (D) Efflux of [^{3}H]-mitoxantrone in the absence and presence of inhibitors in NCI-H460/MX20 cells.

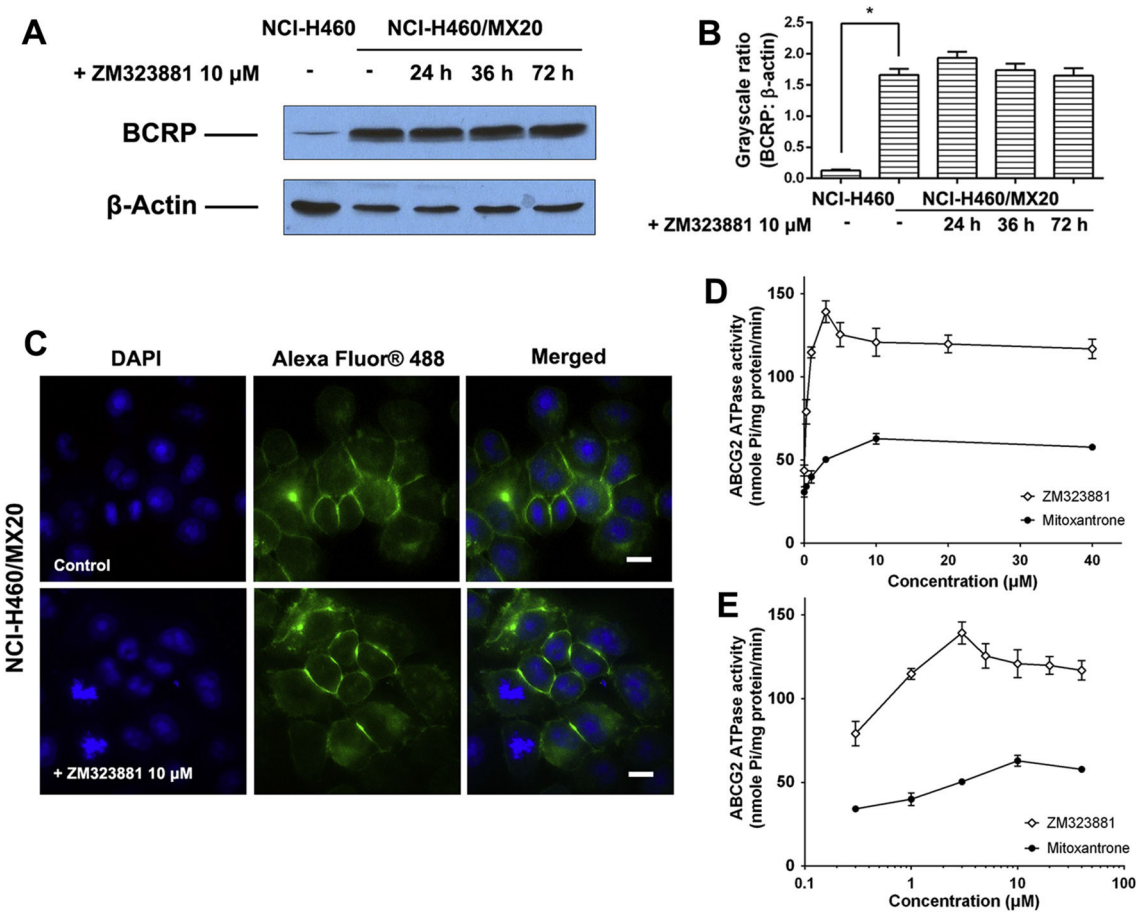

Fig. 4.

(A). The effect of ZM323881 at 10 μM on the expression levels of BCRP in NCI-H460/MX20 cells. (B) Quantitative analysis of effects of ZM233881 at 10 μM on BCRP expression. (C) The effect of ZM323881 at 10 μM on the subcellular localization of BCRP in NCI-H460/MX20 cells. Scale bar, 10 μm, DAPI (blue) counterstains the nuclei. Effects of ZM323881 and mitoxantrone (0–40 μM) on the BCRP ATPase activities. Concentrations of ZM323881 and mitoxantrone are plotted at (D) linear or (E) log scale (For interpretation of the references to color in this figure legend, the reader is referred to the web version of this article.).

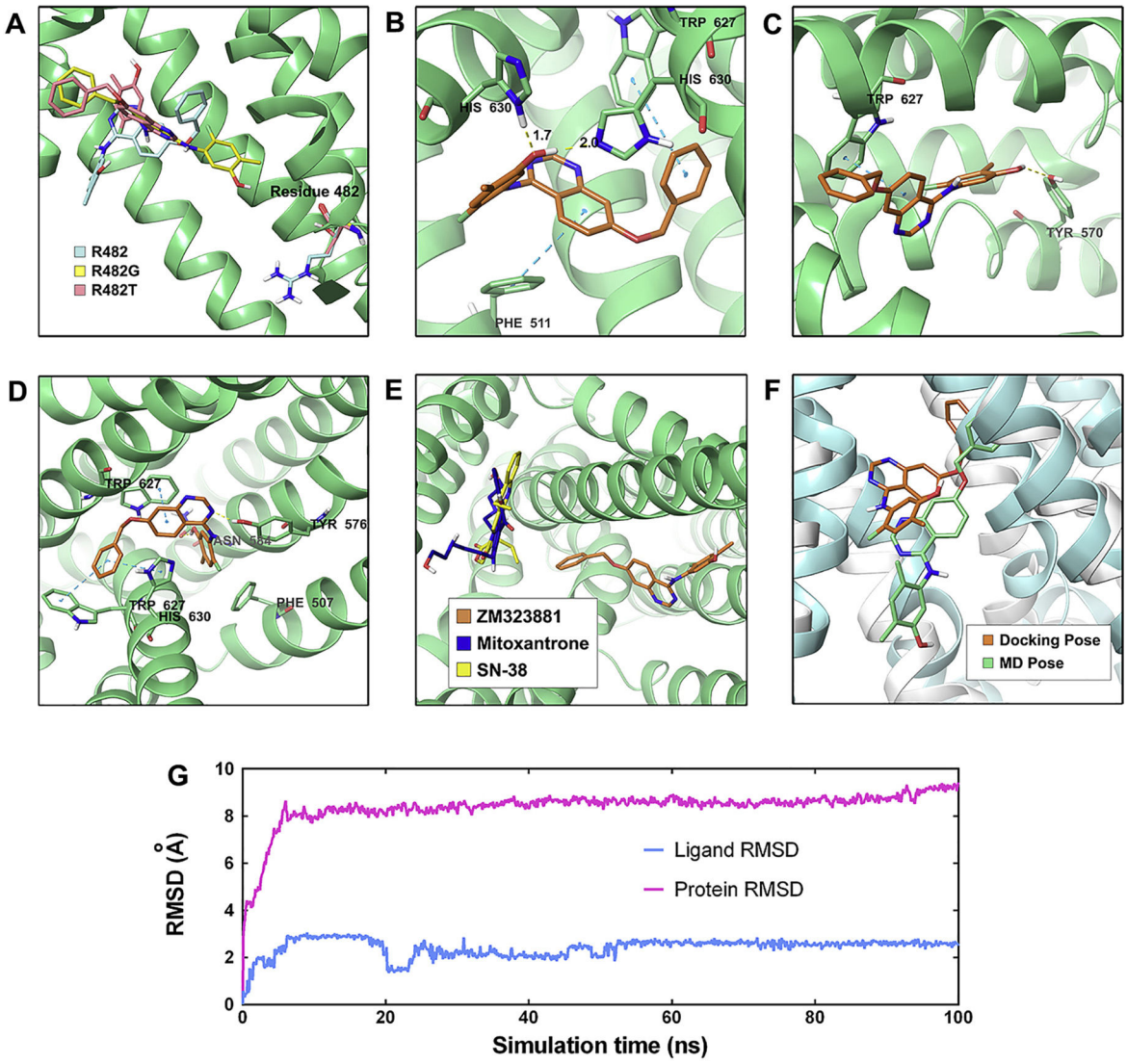

Fig. 5.

(A) Location of ZM323881 and residue 482 in wild-type (R482), R482 G and R482T BCRP internal cavity. (B) The docked conformation of ZM323881 within the binding cavity of wild-type BCRP. ZM323881 and important residues are depicted as sticks with CPK coloring; whereas the carbon atoms in ZM323881 are presented in orange and the carbon atoms in BCRP are presented in green. The dotted cyan lines indicate π-π interaction and the dotted yellow lines indicate hydrogen-bonding interactions. (B) The docked conformation of ZM323881 in R482G BCRP. Color scheme is same as panel (B). (C) The docked conformation of ZM323881 in R482T BCRP. Color scheme is same as panel (D). (E). Location of docked ZM323881 (Carbon: orange), mitoxantrone (Carbon: blue) and SN-38 (Carbon: yellow). (F) Induce-fit docked pose (ligand: organe, protein: white) and MD pose (ligand: green, protein: cyan) of ZM323881. (G) RMSD trajectory of BCRP and ZM323881 in BCRP-ZM323881 complex over the 100 ns simulation run.